Structure Evolution during Gelation at Later Stages of Spinodal Decomposition in Gelatin/Maltodextrin Mixtures

Niklas Lorén, Annika Altskär, and Anne-Marie Hermansson*

SIK—The Swedish Institute for Food and Biotechnology, PO Box 5401, SE-402 29 Göteborg, Sweden

Received April 26, 2001

ABSTRACT: The kinetics of phase separation and gelation in kinetically trapped gelatin/maltodextrin/water gels was studied using confocal laser scanning microscopy (CLSM) and transmission electron microscopy (TEM). The time evolution of the morphology was followed by CLSM during temperature quenches from 60 °C to between 1 and 40 °C. The maltodextrin concentration was varied between 2.25% and 7.5% (w/w), and the gelatin concentration was held constant at 4% (w/w). Spinodal decomposition, self-similar growth, percolation-to-cluster transition, coalescence, and diffusion of maltodextrin inclusions were observed during the progress of gelation. The start and completion of these processes, the onset of phase separation, and the relative rates of phase separation and gelation were found to determine the morphology. The characteristic wavelength showed a crossover in its growth rate power law from one-third to one in a slowly gelling, near-symmetric system. Droplet and bicontinuous morphologies were observed in off-symmetric and near-symmetric quenches, respectively. Secondary phase separation occurred at low temperatures and near-symmetric composition. Partial coalescence and contracted flocculation were observed during the progress of gelation. Stereological measurements showed that the size of maltodextrin inclusions increases and that the volume fraction decreases with increasing quench temperature. In addition, the number of the maltodextrin inclusions decreases with increasing quench temperature.

Introduction

Many mixed biopolymer systems phase separate in aqueous solution and have one component that gels during a thermal quench. Previous work has shown that the morphology of these mixed biopolymer systems depends on the relative rates of phase separation and gelation.[1−3] Incompatible systems unperturbed by gelation will phase separate, equilibrating concentrations and phase volumes. Thereafter, the morphology coarsens by self-similar growth, coalescence, and/or Ostwald ripening and ultimately results in bulk phase separation and creaming. In contrast, incompatible systems that have been quenched to temperatures below the gelation temperature of one of the components will start to gel, which subsequently decreases the mobility, slows down the coarsening, and inhibits phase separation. Finally, gelation will kinetically trap the mixed biopolymer system in a nonequilibrium state. The kinetics of phase separation[4,5] and the kinetics of gelation will determine the morphology of mixed biopolymer systems. Knowledge of the time evolution of the morphology in phase-separated biopolymer systems in relation to the progress of gelation at different compositions and quench temperatures is crucial for an understanding of the morphology generated and the material properties. This work deals with the kinetics of phase separation and the coarsening of the morphology in the late stages of spinodal decomposition in relation to the progress of gelation in gelatin/maltodextrin gels at different experimental conditions using dynamic measurements of the time evolution of the morphology.

Recent work on gelatin/maltodextrin gels using simultaneous optical rotation and turbidity measurements, confocal laser scanning microscopy (CLSM), transmission electron microscopy (TEM), and rheology has shown that the conformational ordering of gelatin[2] gives an extra incentive toward phase separation and shifts the onset of phase separation forward. It was also found that a certain degree of elasticity was needed to trap the morphology. The temperature of phase separation in relation to the gelation temperature in kinetically trapped gelatin/maltodextrin gels was shown to determine the size of the discontinuous maltodextrin inclusions.[3] The size of the maltodextrin inclusions decreases, and the interfacial area between the phases increases with increasing cooling rate.[6] The relative kinetics of gelation and phase separation determined the completeness of the phase separation and the amount of small maltodextrin inclusions trapped in the gelatin phase.

Related studies of the kinetics of phase separation in relation to the progress of the gelation have been done in other biopolymer systems. The kinetics of simultaneous phase separation and gelation in solutions of gelatin and dextran has been studied using light scattering and phase contrast microscopy.[1] Quenches near the critical point were done to temperatures both below and above the gelation temperature of gelatin. Above the gelation temperature, the solution phase separated through spinodal decomposition, and a mottled morphology formed. This then relaxed into droplets that grew with time through coalescence. Below the gelation temperature, phase separation was influenced by the gelation, and in the end, the bicontinuous morphology was frozen in by the gelation process. Studies of the kinetics of spinodal decomposition in gelling gelatin/water/methanol mixtures showed that the final domain size decreases with increasing quench depth and that the mixtures become kinetically trapped by gelation in a nonequilibrium state.[7] In addition, it was found that the relative magnitude of the time scales[8] for phase separation and gelation determined the morphology. Numerical studies have predicted that phase separation

* To whom correspondence should be sent.

10.1021/ma010722q CCC: $20.00
Published on Web 10/04/2001

promotes gelation[9] and that gelation slows down domain growth in the late stages of phase separation.[10]

Dynamic measurements of the time evolution of the morphology of gelling water-in-water emulsions have been scarce until now. However, the time evolution of phase-separating synthetic polymer systems has been observed in two dimensions using polarized light microscopy[11] and in three dimensions[12,13] using CLSM. TEM and CLSM in combination with light scattering have been used to demonstrate the morphological time evolution of a near-critical system during spinodal decomposition.[14]

The coarsening of the microstructure in the late stages of spinodal decomposition involves self-similar[15] growth, percolation-to-cluster (PTC) transition,[16] coalescence,[17] and diffusion after the gelation. Self-similar growth in critical[18] and off-critical[18−20] polymer systems has been studied experimentally[21,22] and theoretically.[23,24] The domain growth obeys the scaling law $L(t) \sim t^{\alpha}$, where $L(t)$ is the characteristic domain size and t is time. Three growth regimes have been established using dimensional analysis:[25] the diffusive ($\alpha = {}^1/_3$), the viscous hydrodynamic[26] ($\alpha = 1$), and the inertial hydrodynamic[27] ($\alpha = {}^2/_3$) regimes. Different time dependencies of self-similar growth have been found in both biopolymer and synthetic polymer systems. The time dependence in the gelatin/dextran[1] system was t^1 above the gelation temperature and $t^{1/3}$ below. After the breakup of the bicontinuous microstructure into a droplet morphology through the PTC transition, the domains grew through evaporation−condensation (Lifshitz−Slyozov−Wagner)[28,29] or coalescence. Transportation of droplets and collisions leading to coalescence can be induced by Brownian motion,[30] concentration gradients,[31] or collision-induced collision.[32]

The main objective of the present work was to use CLSM to examine the mechanisms underlying the morphologies generated in different parts of the phase diagram by following the time evolution of the morphology during phase separation and the progressing gelation in gelatin/maltodextrin gels. The time evolution of the morphology and the final morphology will be discussed according to existing theories on phase separation mechanisms, coarsening, and coalescence. Special emphasis will be given to the morphology in later stages of phase separation in relation to the progress of gelation, using TEM as a complementary technique. It will be demonstrated that quenching to different temperatures and varying composition both have an impact on the size and phase volumes of microstructural features and the type of morphology in the final gel structure.

Experimental Methods

Materials. The gelatin sample, type LH, 240 Bloom, used[2,3] was provided and characterized by Systems Bio-Industries, Research Centre, Baupte, F-50500 Carentan, France. It has an isoelectric point of pH 4.7. The number-average molecular weight was 83.3 kDa, and the mass-average molecular weight was 146 kDa. The maltodextrin quality used was Paselli SA2, provided by Avebe, 9607 PT Foxhol, and characterized by Unilever Research Laboratory, Sharnbrook, UK. It is an enzymatically converted potato starch with a pH between 5.5 and 7.0 and has a dextrose equivalent (DE) between 2.3 and 2.8 g/100 g. From the DE value, the number-average molecular weight can be estimated to be about 9 kDa.

The maltodextrin was made fluorescent by covalent binding[3,33,34] of RITC (rhodamine B isothiocyanate). Details about the mixing of the gelatin and the maltodextrin components can be found elsewhere.[3] After transferring the mixed solution to the CLSM, the sample was stabilized for a few minutes at 60 °C and then cooled from 60 °C to different quench temperatures (T_q) at a cooling rate of 30 ± 2 °C min^{-1}.

CLSM and Image Processing. The CLSM system consists of a Leica TCS 4D confocal laser scanning microscope (Heidelberg, Germany) equipped with a Linkam TMS 92 heating-and-cooling table. The emission maximum at 488 nm of an argon−krypton laser was used as the light source. Based on the size of the dispersed phase, a microscope objective having a magnification of 63 times and computer zooming factors of 1.98× and 3.97× were used. The signals from the sample above 590 nm were collected with a tritc filter, and eight scans were averaged during the creation of an image.

The recording of images started immediately at 60 °C, after which the temperature quenches began. Two different scanning modes were used, normal and fast, giving image recording times of 3.77 and 1.43 s, respectively. The fast scanning mode was used for most samples. The number of images recorded varied between 60 and 300 depending on the expected kinetics of phase separation and gelation. The position of the confocal plane was held constant throughout the whole sequence of image recording. All images were taken at a depth of 50 μm inside the sample to avoid surface effects, but the depth varied to some extent (less than 5 μm) since a sample could swell or shrink during the complete image sequence.

The images were transferred to a SUN Ultra1 workstation and stored on a hard disk. A Contextvisions microGOP 2000/S (Linköping, Sweden) contextual image analysis system was used to create binary images, mainly by image enhancement using GOP operations and thresholding, and to make stereological measurements.

Measurement of the Characteristic Wavelength. The characteristic wavelength, Λ_{max}, was measured in order to quantify the time dependence of the self-similar growth of the continuous maltodextrin phase according to the scaling law $L(t) \sim t^{\alpha}$, where $L(t)$ is the distance between the maximum of the growing waves and t is time. The characteristic wavelength was measured manually by drawing a line from the middle of one part of the maltodextrin phase, perpendicular to the interface between the gelatin phase and the maltodextrin phase, to the middle of the next part of the maltodextrin phase. Twenty such lines were drawn in each micrograph, and the number-average of the length of each line was taken as the characteristic wavelength for that particular micrograph. The logarithm of the wavenumber, $q_{max} = 2\pi/\Lambda_{max}$, was plotted against the logarithm of the time after the onset of phase separation. The slope is equal to the negative α exponent. In a forthcoming paper, the fast Fourier transform (FFT) will be used to calculate the growth rate at various quench temperatures.

Stereological Image Analysis. A model-based approach to stereology was used because the samples were isotropic. Two stereological measures were calculated: the volume-weighted mean volume (also called the star volume) and the volume fraction. Seven images from each sample at different locations were used to calculate the volume-weighted mean volume and the volume fraction. The number of particles counted in each measurement varied between 120 and 330, and the coefficient of error ranged between 0.06 and 0.15. To obtain an unbiased measure, the two-dimensional counting rule was applied to the images,[35] and this meant that a measure frame was introduced. The formula

$$V^* = \frac{\pi}{3}\bar{l}_0^{\,3}$$

was used to estimate the volume weighted mean volume,[36] where l_0 is the intercept length, i.e., the length from one boundary through a random point to the other boundary.

The volume fraction is related to the area fraction through the Delesse principle[37] $V_V = A_A$, where V_V is the volume fraction and A_A the area fraction. The area fraction was measured in the CLSM images.

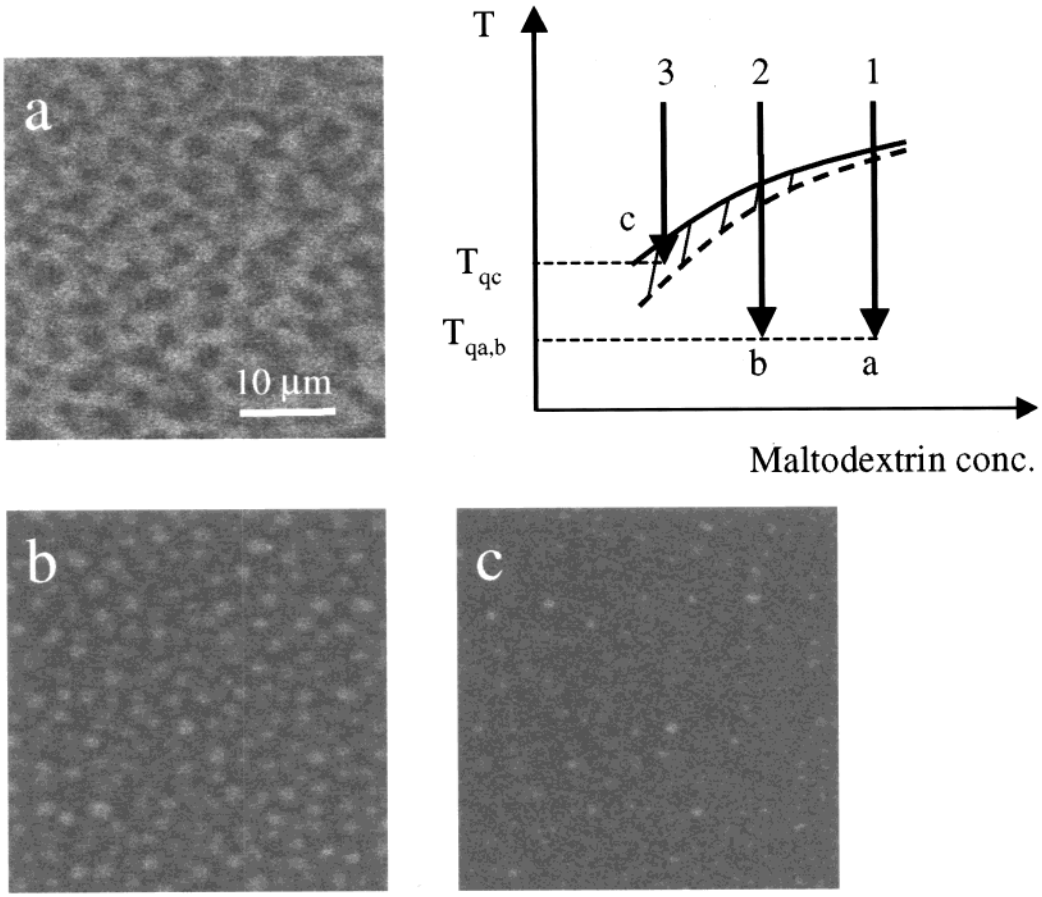

Figure 1. A purely schematic temperature−composition phase diagram of the ternary gelatin/maltodextrin/water system showing different quenches routes. The microstructural development at early stages of the phase separation corresponding to the different quench routes at constant 4% (w/w) gelatin concentration are shown as CLSM micrographs: (a) spinodal decomposition, 7.3% (w/w) maltodextrin, 1 °C, 5 s after the onset of phase separation as observed by CLSM; (b) spinodal decomposition, 5% (w/w) maltodextrin, 1 °C, 8 s; (c) not determinable by CLSM, 3% (w/w) maltodextrin, 20 °C, 45 s.

Transmission Electron Microscopy (TEM). Small pieces of gels were doubled-fixed in 2% glutaraldehyde and 2% OsO_4. Samples were dehydrated in a grade ethanol series, transferred to propylene oxide, stepwise propylene oxide/polybed, and then embedded in polybed 812 and polymerized. Thin sections of ~70 nm were cut on a diamond knife and double-stained with uranyl acetate and lead citrate. The sections were examined in a TEM, LEO 906e, at an accelerating voltage of 100 kV.

Results and Discussion

Early Stages of Phase Separation Following Different Quench Routes. The gelatin/maltodextrin/water system is known to obey an upper critical solution temperature (UCST) behavior, which means that it starts to phase separate during a thermal cooling step into the incompatibility region. The starting point of all experiments in this work is a homogeneous solution well above the temperature of phase separation. The maltodextrin concentration was varied between 2.25% and 7.5% (w/w) and the quench temperature (defined as the end temperature of the quench) between 1 and 40 °C. The gelatin concentration was kept constant at 4% (w/w).

A section of the schematic ternary gelatin/maltodextrin/water temperature−composition phase diagram at constant gelatin concentration, obeying segregative[38] phase separation, is shown in Figure 1. The one-phase region above the binodal is drawn as a solid line, and the metastable region between the binodal and the spinodal is drawn as a broken line. The compositions studied in this work are located in a region of the ternary phase diagram[39] that contains no critical points, and all solutions enter the metastable region before they reach the unstable region during a thermal step.

Three different quench routes are shown in the schematic phase diagram in Figure 1. The growth of a bicontinuous microstructure at early stages of phase separation corresponding to quench route 1 can be seen in Figure 1a. The mottled microstructure shown in micrograph a is typical of spinodal decomposition. All samples between 6% and 7.5% (w/w) maltodextrin concentration exhibit the mottled microstructure during some part of their time evolution.

The growth of discontinuous microstructures at early stages of phase separation corresponding to quench routes 2 and 3 can be seen in micrographs b and c of Figure 1, respectively. The morphology obtained by quench route 2 is also attributed to spinodal decomposition. The samples that phase separated through quench route 3 shows a nucleation-and-growth-like behavior.

The main objective of this work is to show how the maltodextrin concentration, quench routes 1−3, and the quench temperature, $T_{qa,b,c}$, and thereby the quench depth, influence the phase separation mechanism, the kinetics of phase separation, and the kinetics of gel formation. The effect of the mechanism and the kinetics on the morphology of the gelatin/maltodextrin/water system will also be demonstrated.

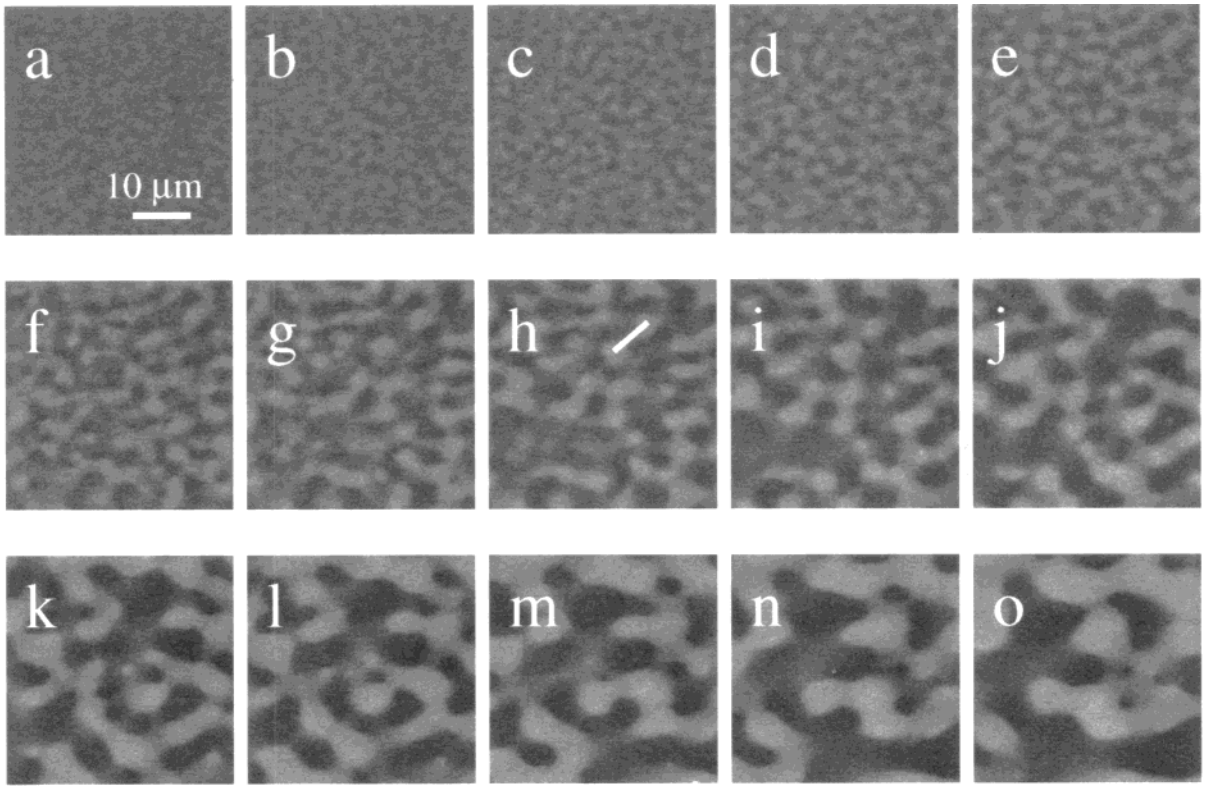

Figure 2. CLSM micrographs showing a quench of 4% (w/w) gelatin and 7.3% (w/w) maltodextrin concentration from 60 to 30 °C, according to quench route 1. The time between every micrograph is 2.86 s.

Time Evolution of the Morphology. The morphology can evolve in at least two different ways depending on the composition. Mixtures having critical[40] composition will remain bicontinuous even in the late stages of spinodal decomposition. In contrast, in off-critical[41] mixtures, phase separating through spinodal decomposition, the minority phase can no longer maintain its continuous morphology as phase separation proceeds, whereas the system undergoes PTC transition and a droplet morphology forms.

The growth and pattern formation of spinodal decomposition may be classified into at least three regimes: (a) early stage, (b) intermediate stage, and (c) late stage.[42,43] In the early stage, described by the Cahn−Hilliard theory,[44] the spatial concentration fluctuations start to grow in amplitude at a certain energetically most favorable wavelength, independent of time. The intermediate stage begins when the peak spatial concentration fluctuations reach the coexisting concentration. It is characterized by increased wavelength, which is the same as increased size and separation of the domains and decreased interfacial width. The early and intermediate stages in spinodal decomposition are difficult to separate using CLSM. In the late stage of spinodal decomposition, the interfacial width has nearly reached its equilibrium distance, and the domains continue to increase in size through self-similar growth in order to reduce the interfacial free energy of the system.

Quench Route 1. The time evolution of the microstructure of a quench from 60 to 30 °C, which is the gelation temperature of gelatin, is shown in Figure 2. Gelation does not affect the evolution of the morphology of this system because the gelatin gels very slowly at 30 °C. The mottled morphology displayed in the whole sequence in Figure 2 is taken as evidence that the phase separation proceeds through spinodal decomposition. Mixtures with time evolutions similar to the sequence shown in Figure 2 with a bicontinuous morphology are termed (near-) symmetric quenches. The term symmetric refers to the middle of the tie-line, which is approximately estimated from the temperature-dependent phase diagram[45] of related gelatin/maltodextrin/water systems.

Micrograph a of Figure 2 shows the onset of phase separation 50 s after the beginning of the quench. The onset of phase separation as observed by CLSM appears quickly and over the whole sample at the same time. The total time for the entire sequence shown in Figure 2 is 41.5 s. The bright part of the CLSM micrographs is the maltodextrin phase and the dark part the gelatin phase. Contrast differences caused by concentration fluctuations define the onset of phase separation. These differences can be observed in micrographs a and b for this system. It can be seen that the contrast between the gelatin phase and the maltodextrin phase increases and that the interfacial width between the gelatin phase and the maltodextrin phase decreases from micrographs a to k. This means that the difference in maltodextrin concentration between the gelatin phase and the maltodextrin phase increases with time until it has reached the equilibrium coexistence concentration (∼ micrograph k) of the system.

Another important feature of the whole sequence in Figure 2 is the increase in the characteristic wavelength of the system with time through self-similar growth. This means that the diameter of each part of the mottled microstructure and the distance between each part of this structure increase with time. Figure 3 shows the logarithm of the wavenumber (q_{max}) as a function of the logarithm of the time after the onset of phase separation for a part of the sequence shown in Figure 2. For

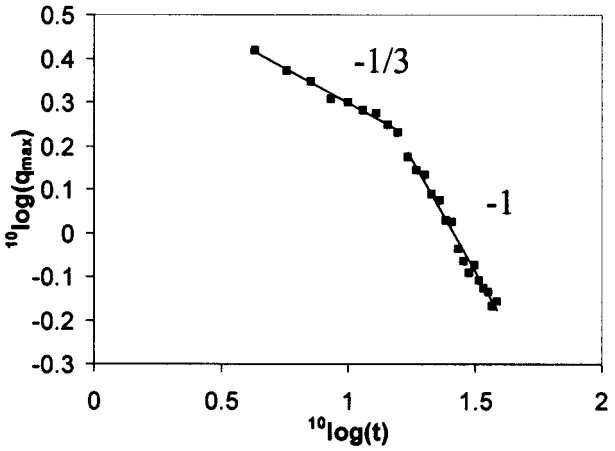

Figure 3. Manual measurement of the α exponent in the scaling law at 4% (w/w) gelatin and 7.3% (w/w) maltodextrin concentration, quench to 30 °C. The straight lines represent least-squares estimates of the slope of the data.

example, the points in Figure 3 at log t equal to 0.63 and 1.59 represent the measurements of the characteristic wavelength in micrographs a and m in Figure 2, respectively. One example of this measurement is shown as a white line in micrograph h in Figure 2. The characteristic wavelength varies between 2.4 and 9.0 μm, and the time varies from 4.3 to 38.6 s after the onset of phase separation in Figure 3. The standard deviation of q_{max} was approximately a tenth of its value. The measurement was stopped at log t equal to 1.59 because the number of wavelengths was too small (for ergodic reasons).

The slopes of the linear curves in Figure 3 are equal to the negative α exponents in the scaling law $L(t) \sim t^{\alpha}$. They were determined by least-squares fits to the data. Figure 3 shows that the mottled microstructure grows at two different growth rates. The growth rate in the first part between log t is equal to 0.63 and 1.20 has an α exponent equal to $^1/_3$. The first part of the evolution of the microstructure is thus governed by diffusion. The rate of growth changes at log t equal to 1.20 (16 s after the onset of phase separation), i.e., between micrographs d and e in Figure 2. In the second part, the mottled microstructure grows at a rate proportional to t^1, which means that the α exponent is equal to one. This exponent coincides with the theoretical predictions of Siggia.[26] The capillary pressure involved in the mottled microstructure drives the growth of the characteristic wavelength. Parts of the mottled microstructure with a thick diameter have a lower capillary pressure than parts with a thin diameter. The pressure gradient may cause Poiseille flow from the thin parts toward the thick parts of the mottled microstructure, which results in a growth rate proportional to t^1 owing to scaling arguments. This means that the second part of the evolution of the microstructure is governed by hydrodynamic flow. The observed crossover from an α exponent of $^1/_3$ to 1 in the gelatin/maltodextrin system has also been observed in other systems such as unstable mixtures of silica spheres (coated with stearyl alcohol) and PDMS[46] and mixtures of aggregated whey protein colloids with exocellular polysaccharides.[47] The resulting morphology will be a bicontinuous microstructure because the quench that is done is close to the middle of the tie-line in question, and the volume fractions are within the percolation threshold. Gelation proceeds rather slowly[48] at 30 °C but will finally trap the system in a bicontinuous microstructure.

Quench Routes 2 and 3. Quench routes 2 and 3 are termed off-symmetric, and they always gives rice to discontinuous microstructures. The time evolutions of the microstructure of two quenches from 60 to 5 °C, according to quench route 2, are shown in Figure 4a,b. The onset of phase separation, shown in micrographs a1 and b1, can be seen as small, irregular concentration fluctuations. The concentration fluctuations are much larger for the 6% (w/w) maltodextrin mixture (micrograph a1) as compared with the 4% (w/w) maltodextrin mixture (micrograph b1). The characteristic wavelength of the indistinct mottled maltodextrin phase of the 6% (w/w) maltodextrin system shown in micrograph a2 increases quickly with time. This results in an increase in the size of the maltodextrin phase. In addition, the difference in maltodextrin concentration between the maltodextrin phase and the gelatin phase increases. This is shown by the increased contrast between the dark gelatin phase and the bright maltodextrin phase. The mottled maltodextrin phase then relaxes to smaller discontinuous domains through the PCT transition shown in micrograph a3. These maltodextrin domains form spherical maltodextrin inclusions in order to minimize the interfacial free energy.

The 4% (w/w) maltodextrin system evolves differently with time as compared to the 6% (w/w) maltodextrin system. The concentration fluctuations in the 4% (w/w) maltodextrin system shown in micrograph b1 relax directly to bright, evenly sized, nearly spherical and randomly distributed maltodextrin inclusions that develop quickly and simultaneously in the whole sample. These inclusions grow in size, and the contrast between the gelatin phase and the maltodextrin phase increases simultaneously with time as can be seen in micrographs b1−b4. These observations are normally attributed to off-critical spinodal decomposition[18,49] and provide strong evidence of spinodal decomposition because the inclusions are expected to be strongly correlated through the depletion layers in the unstable region.[23,50] The mottled microstructure formed by the early stages of spinodal decomposition breaks up into discontinuous domains through a PTC transition at very early times before these domains are observable in the CLSM due to limited resolution and the necessary contrast differences between the phases. Computer simulations of off-critical blends[18] have shown a similar breakup of the microstructure at early stages of spinodal decomposition. In addition, neither the quenches at 4% (w/w) nor those at 6% (w/w) maltodextrin concentration show any effect of the quick passage through the metastable region on the time evolution of the morphology, owing primarily to the finite kinetics of nucleation and the polydispersity of gelatin and maltodextrin.

The discontinuous maltodextrin inclusions formed by the PTC transition continue to grow in size by coalescence between the maltodextrin inclusions, shown in micrographs a4 and b4, for both the 6 and the 4% (w/w) maltodextrin systems. The rate of coalescence is slowed owing to the onset of gelation and is finally impeded by the gelatin network. Thus, the coarsening of the microstructure by coalescence can only proceed unimpeded for a short period. The length of this period is dependent on the start of the coalescence process in relation to the progress of gelation and can proceed longer for the 6% (w/w) maltodextrin system than for

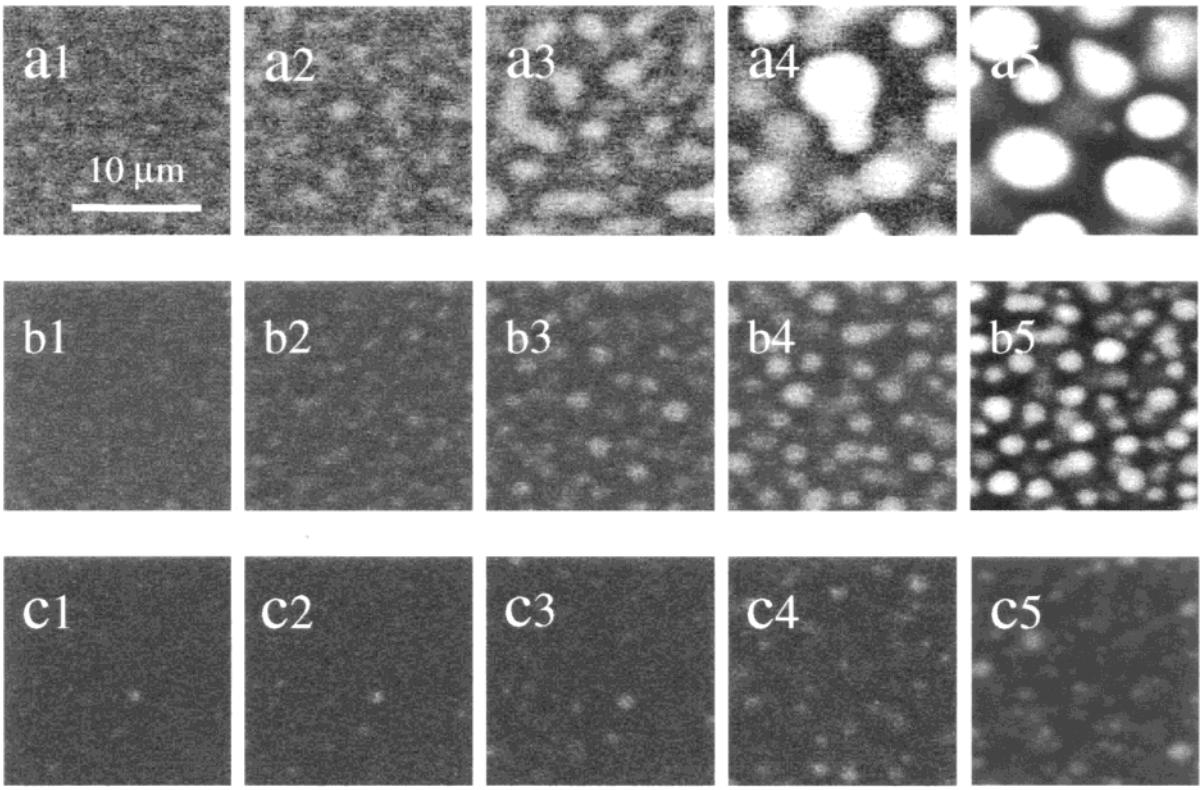

Figure 4. CLSM micrographs showing two quenches from 60 to 5 °C, according to quench route 2, and one quench from 60 to 20 °C, according to quench route 3. All samples have 4% (w/w) gelatin concentration. 6% (w/w) maltodextrin: (a1) 71 s after quench start; (a2) 74 s; (a3) 76 s; (a4) 90 s; (a5) 110 min, 4% (w/w) maltodextrin: (b1) 85 s after quench start; (b2) 88 s; (b3) 93 s; (b4) 113 s; (b5) 33 min, 3% (w/w) maltodextrin: (c1) 280 after quench start; (c2) 300 s; (c3) 330 s; (c4) 475 s; (c5) 24 min.

the 4% (w/w) maltodextrin system. Finally, the microstructures are trapped at a nonequilibrium stage by gelation. The final resulting microstructures are shown in micrographs a5 and b5.

The time evolution of the microstructure of a quench from 60 to 20 °C, according to quench route 3, is shown in Figure 4c. The maltodextrin inclusions appeared at different times during the evolution of the microstructure. They vary in size and grow almost independently, and they are few. These observations are normally attributed to the nucleation and growth mechanism.[50] However, it is known that the transition between spinodal decomposition and nucleation and growth is gradual and depends on the interaction range and quench depth.[51]

Coarsening in the Late Stage of Phase Separation. There are several coarsening processes, such as hydrodynamic flow, diffusion, self-similar growth, and coalescence, through which morphology can grow. The common feature of these processes is that they all invoke some kind of transport of material in the system. The transport of materials can occur between the two phases or inside the phases. The driving force for the transportation of material can be thermodynamic gradients, such as concentration gradients, osmotic pressure, or interfacial free energy, or induced flow such as from convection or shear. The transport is dependent on the mobility of the materials in the solution and the friction between these. In addition, structures such as networks, pores, channels, or membranes can affect the transport.

Coarsening While Gelation Proceeds. The coarsening of off-symmetric gelatin/maltodextrin/water systems in the late stages of spinodal decomposition with time during the progress of gelation is schematically shown in Figure 5. Phase separation proceeds through the different stages of spinodal decomposition, and the system then relaxes to discontinuous maltodextrin inclusions through the PTC transition. These inclusions start to grow through coalescence between the maltodextrin inclusions in the solution. However, if the solution is quenched to a temperature below 30 °C, i.e., below the gelation temperature of gelatin, the gelation will have an impact on the phase separation and the coarsening of the morphology. Gelation can stop the coalescence between the maltodextrin inclusions either by trapping the coalescence at an intermediate stage where the inclusions have partly coalesced or by forming a thin lamella between the inclusions that impedes the coalescence process. These processes are shown in Figure 5 and are called partial coalescence and contracted flocculation, respectively. Ultimately, gelation

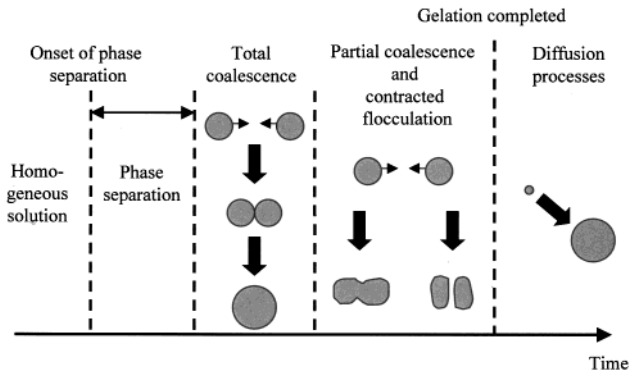

Figure 5. Schematic representation of the different stages of coalescence occurring during the progress of gelation with time.

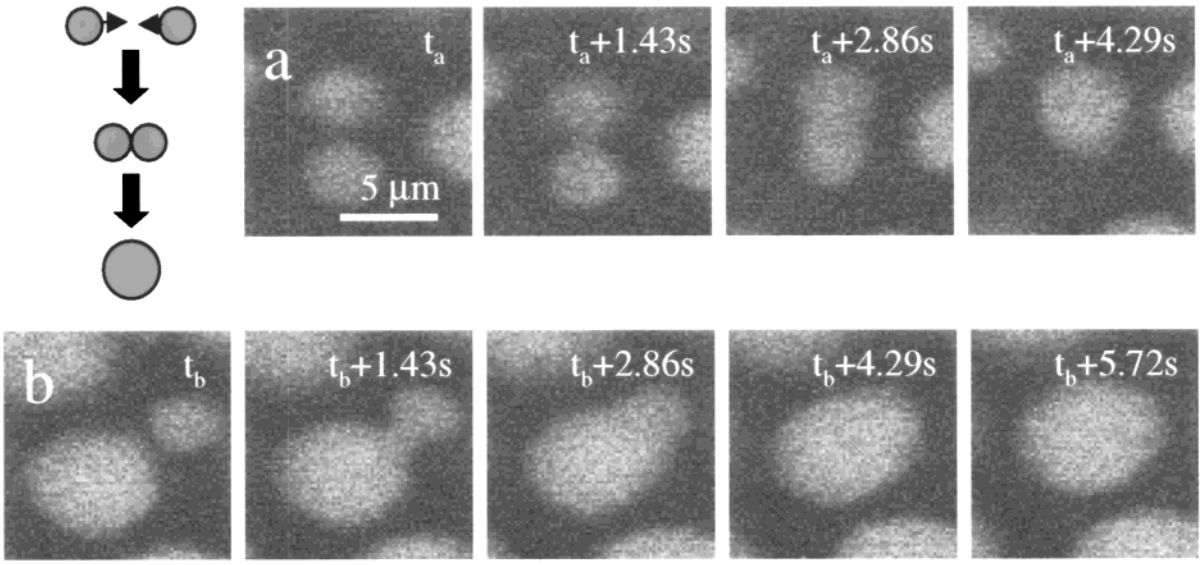

Figure 6. CLSM micrographs showing two examples of total coalescence at 4% (w/w) gelatin and 6% (w/w) maltodextrin, quenched to 25 °C: (a) $t_a = 140$ s after the start of quenching; (b) $t_b = 215$ s. The time between every micrograph is 1.43 s.

traps the microstructure and only diffusion processes remain active.

Coalescence. Coalescence between maltodextrin inclusions can be observed in all samples in the experimental design except at low (2.25% (w/w)) and high maltodextrin concentrations (7.3% and 7.5% (w/w)). The phase separation at low maltodextrin concentrations occurs at a viscosity high enough to prevent coalescence, while the microstructure is bicontinuous at high maltodextrin concentrations.

The CLSM micrographs in Figure 6 show two examples of coalescence between pairs of maltodextrin inclusions quenched to 25 °C at different times after the start of quenching. Sequences a and b were taken 140 and 215 s, respectively, after the start of the quench. Hence, the mobility is lower; i.e., the viscosity is higher in sequence b as compared to sequence a, owing to the progress of gelation.

First, the maltodextrin inclusions approach each other to reach a distance of less than 1 μm. Second, the continuous gelatin phase between the inclusions is removed, the interstitial remaining continuous gelatin phase ruptures, and a "bridge" of maltodextrin connects the two inclusions. The gelatin phase is then ejected from between the two coalescing maltodextrin inclusions as a result of the high curvature of the newly formed interface.[52] Finally, the maltodextrin inclusion takes on a spherical shape, and its volume is equal to the sum of the volumes of the two original inclusions. All these steps are in agreement with existing theories about the coalescence process in polymer/polymer systems.[53,54] The coalescence time, from the beginning to the end of the coalescence process shown in sequence a in Figure 6, was approximately 4 s.

Sequence b in Figure 6 shows coalescence between two spherical maltodextrin inclusions of different sizes. The coalescence between the two maltodextrin inclusions proceeds in a similar way as the one shown in sequence a. However, the coalescence time for sequence b was approximately 6 s. The increase in the viscosity of the ejected phase between the inclusions in sequence b increases the coalescence time.[52] This time increase depends on the progress of gelation. Nevertheless, some part of the increase in time can be attributed to the increased radius of one of the inclusions. In addition, it is known that coalescence broadens the size distribution of the inclusions,[55] which can result in an alternation of the coalescence time. Another effect of gelation can be seen in the last three CLSM micrographs in sequence b. They demonstrate that the relaxation toward an energetically favored spherical shape in the last micrograph takes much longer time than the relaxation in sequence a.

The approach of the maltodextrin inclusions toward each other in the gelatin/maltodextrin system is probably caused by the gradient-induced coupling mechanism,[31] because the volume fraction is above 0.20, and the evaporation condensation mechanism[28,29] and the Brownian coagulation mechanism[30] are active only at volume fractions below 1/12.[31] However, recent experiments[56] have shown that Brownian drop motion can be active at volume fractions between 0.1 and 0.3. In addition, the collision−collision-induced coalescence mechanism[32] was occasionally observed. Droplets experiencing collision have a higher probability of a subsequent collision, owing to the strong coupling of the velocity and diffusion fields after the coalescence.

Partial Coalescence and Contracted Flocculation. As gelation proceeds with time, the mobility of the materials in the solution decreases. Thus, the number of coalescence events becomes fewer. The coalescence time increases, and the relaxation of the maltodextrin inclusion toward a spherical shape becomes impeded by gelation, making the inclusions only partially coalesce. Transmission electron micrographs a and b in Figure 7 clearly show partial coalescence in a gelatin/maltodextrin solution quenched to 5 °C.

Contracted flocculation can be seen in transmission electron micrographs c and d as the deformed maltodextrin inclusions having a thin lamella of gelatin between each other. They are formed when two maltodextrin inclusions have come close to one another in the first step in the coalescence process. No "bridge" between the maltodextrin inclusions can develop, however, because gelation has formed a thin gelatin lamella between the inclusions that impedes the bridge building and thereby also impedes the coalescence between the maltodextrin inclusions. The deformed shape of the

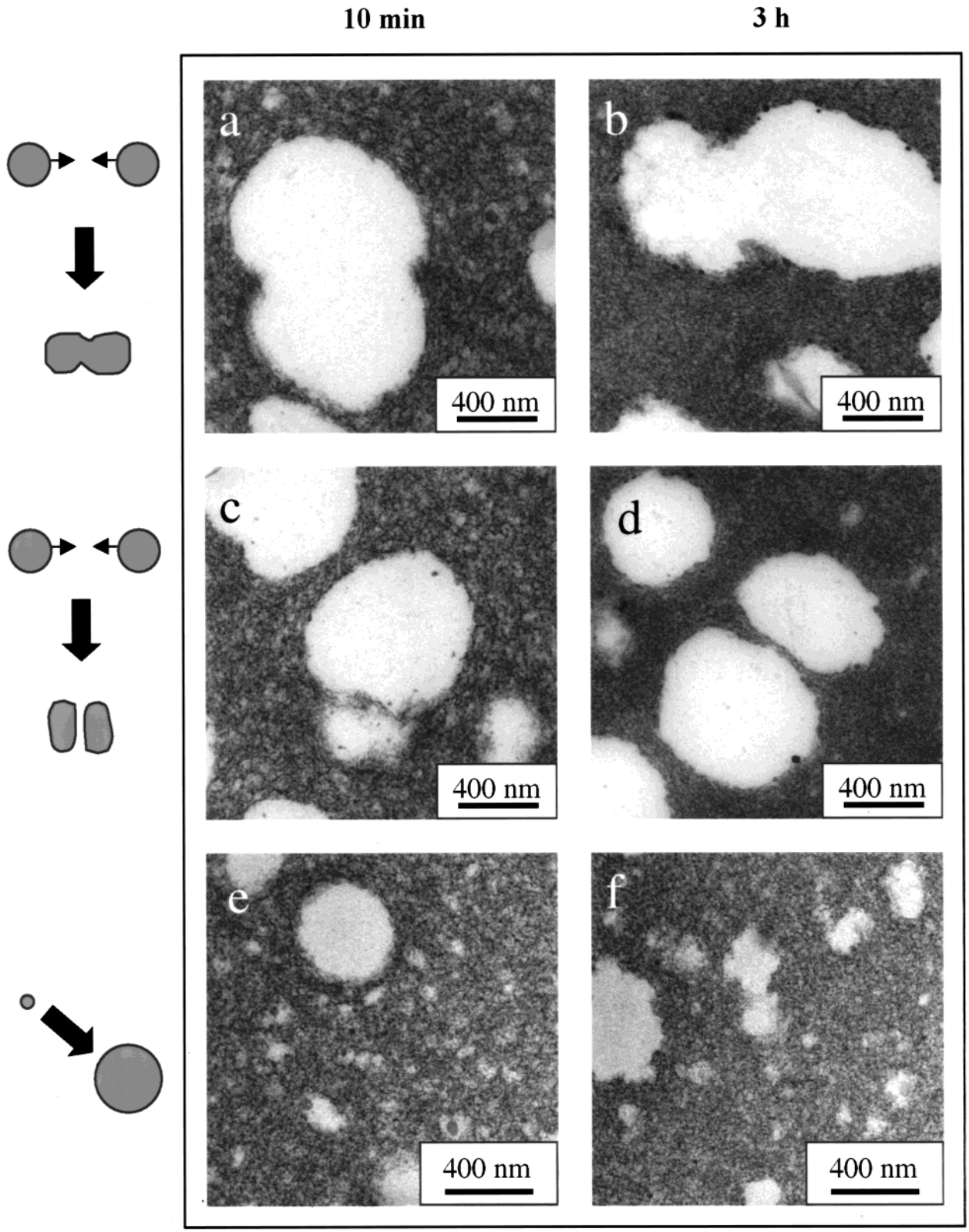

Figure 7. TEM micrographs showing partial coalescence, contracted flocculation, and migration of maltodextrin inclusions. All micrographs have 4% (w/w) gelatin concentration: (a) partial coalescence, 3% (w/w) maltodextrin concentration, quenched to 5 °C, 10 min; (b) partial coalescence, 3% (w/w) maltodextrin, 5 °C, 3 h; (c) contracted flocculation, 3% (w/w) maltodextrin, 5 °C, 10 min; (d) contracted flocculation, 3% (w/w) maltodextrin, 5 °C, 3 h; (e) migration, 2.25% (w/w) maltodextrin, 5 °C, 10 min; (f) migration, 2.25% (w/w) maltodextrin, 5 °C, 3 h. The scale bar is 400 nm.

maltodextrin inclusions during the partial coalescence and the contracted flocculation are an effect of the increased viscosity of the gelatin phase. Owing to the deformable nature of the inclusions and to the viscosity of the phase between the inclusions, the inclusions deform from their original spherical shapes as the phase between the inclusions is squeezed out from between them.[52,57] This means that low viscosity results in minor deformations of the maltodextrin inclusions during coalescence and that high viscosity results in deforma-

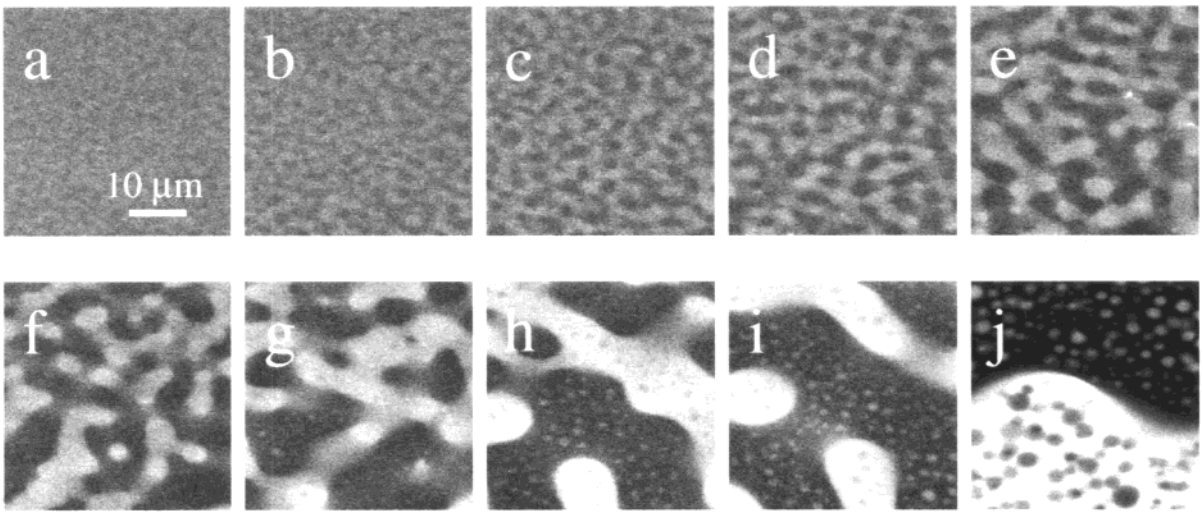

Figure 8. Example of self-similar growth and secondary phase separation at 4% (w/w) gelatin and 7.3% (w/w) maltodextrin concentration, quenched to 1 °C. The time between each micrograph from a to i is 3.8 s. Micrograph j was recorded 12 min after the start of quenching.

tions of the maltodextrin inclusions during partial coalescence and contracted flocculation.

Partial coalescence and contracted flocculation have been observed in all gelatin/maltodextrin systems containing 3%, 4%, 5%, and 6% (w/w) maltodextrin with a quench temperature at or below 20 °C in the experimental design. Examples of partial coalescence and/or contracted flocculation can be seen in CLSM micrographs e and j in Figure 4 as maltodextrin inclusions having a "peanut" or an elongated form. Furthermore, it is important to note that coalescence, partial coalescence, and contracted flocculation all appear to different extents depending on the phase volumes of the phases, the onset of the phase separation, the onset of gelation, and the relative rates of phase separation and gelation.

Diffusion. The fine structure of the morphology after gelation at 5 °C was studied using TEM. Micrographs e and f in Figure 7 show that the gelatin phase is much more homogeneous after 3 h than after 10 min. The gelatin phase contains many more small, irregular maltodextrin inclusions after 10 min than after 3 h. Similar phenomena can be seen in micrographs a−d in Figure 7.

Figure 7 shows strong evidence of a transport of maltodextrin from the gelatin phase to the maltodextrin phase. Here, gelation has trapped the microstructure in a state far from equilibrium. In addition, the boundaries between the gelatin phase and the maltodextrin phase in micrographs e and f are more irregular after 3 h than after 10 min, especially at the large maltodextrin inclusions. They look like large spherical maltodextrin inclusions upon which small maltodextrin inclusions have been stacked. Consequently, the small maltodextrin inclusions trapped in the gelatin network have migrated through this network to the boundary of the larger maltodextrin inclusions. This migration has also been observed in synthetic polymer systems[58] and in computer simulations of phase separation in binary mixtures with a glass-forming component.[59]

Secondary Phase Separation. Secondary phase separation can be observed in the near-symmetric gelatin/maltodextrin/water systems between 6% and 7.5% (w/w) maltodextrin concentrations quenched to temperatures between 1 and 25 °C. Figure 8 shows CLSM micrographs of the time evolution of 4% (w/w) gelatin and 7.3% (w/w) maltodextrin concentration quenched from 60 to 1 °C. The onset of phase separation is shown in micrograph a, 50 s after the start of quenching.

The time evolution of the microstructure is similar to that in the near-symmetric system shown in Figure 2. Small, bright maltodextrin inclusions start to appear in the dark original gelatin phase, however, and small, dark gelatin inclusions begin to arise in the bright original maltodextrin phase in micrograph h in Figure 8. The small inclusions appear quickly in both phases, and the size and the contrast between them and the surrounding phases increase with time. In addition, the maltodextrin inclusions inside the gelatin phase are randomly distributed. The final morphology after trapping is shown in micrograph j. The size of the original maltodextrin phase has increased as have the phases formed in the secondary phase separation. In addition, partial coalescence and/or contracted flocculation of the maltodextrin inclusions can be observed in the original gelatin phase.

Secondary phase separation can emerge through at least four different processes: (a) noninstantaneous temperature changes;[60,61] (b) altered thermodynamic conditions, for example by cross-linking[62] or conformational ordering;[2] (c) mass transfer limitations;[63] (d) rapid hydrodynamic coarsening.[64] Process c is not interesting in the case of the gelatin/maltodextrin system, at least not under the experimental conditions used in this study, because the gelation is too slow and no semipermeable membrane is formed. However, the temperature was decreased by 30 °C/min in our experiments, which means that the solution spent some time in different thermodynamic states during its passage through the phase diagram down to the quench temperature (see Figure 1). In addition, the conformational ordering of gelatin[2] changes the thermodynamic conditions during the thermal quench and gives an extra incentive toward phase separation. These processes can presumably result in a two-stage phase separation process.

Another process interesting for the gelatin/maltodextrin system is rapid hydrodynamic coarsening.[64] In this process, the original phases move faster than the concentration diffusion as a result of hydrodynamic coarsening and do not accompany the concentration

changes, making it impossible to establish local equilibrium. This results in a double quench effect called the interface quench effect.[64] Computer simulations[64] have shown morphology similar to that observed in the gelatin/maltodextrin system in Figure 8. Furthermore, the molecular weight distribution can have an impact on the secondary phase separation because fractions with high molecular weight have a greater ability to phase separate than do fractions with low molecular weight.

Effect of Quench Temperature and Maltodextrin Concentration on the Morphology. The quench depth and the concentration affect the volume fraction and the free energy of mixing and thereby the kinetics of phase separation.[60] The volume fraction is usually assumed to have a major impact on the resulting morphology.[65] In addition, the wavelength selection mechanism[49] in the early stages of spinodal decomposition will result in different characteristic wavelengths depending on the free energy of mixing and the mobility of the system, which can alter the morphology.

Figure 9 shows CLSM micrographs of off-symmetric quenches to 1 and 20 °C. The contrast between the phases is low, and the inclusions are diffuse in micrographs a and b as compared to micrographs c to h because they were recorded at the onset of phase separation as observed by CLSM. The final morphology after the microstructures became kinetically trapped by gelation are shown in micrographs c−h. Micrographs c−h (except d) show spherical, evenly sized, and randomly distributed maltodextrin inclusions, normally indications of spinodal decomposition. In contrast, micrograph d shows maltodextrin inclusions of different sizes and diffuse interfaces that occurred at different times.

The morphology at the onset of phase separation and the final morphology after the trapping show a striking resemblance. The number of maltodextrin inclusions is higher at 1 °C than at 20 °C in Figure 9, and the size of the maltodextrin inclusions is larger at 20 °C than at 1 °C. The early stages of the phase separation are thus important for the final morphology. The deeper quench at 1 °C allows for shorter wavelength fluctuations because of the high free energy penalty associated with sharp concentration gradients.[43] In addition, gelation proceeds faster at 1 °C than at 20 °C, which quickly reduces the mobility and obstructs long wavelength fluctuations. Theoretical work has shown that network elasticity arising from the gelation can suppress long wavelength concentration fluctuations.[66] Any process that can alter the driving force toward phase separation or the mobility of the system can potentially change the energetically most favorable wavelength and thereby the final morphology.

The corresponding stereological measurements of the volume-weighted mean volume and the volume fraction as a function of quench temperature are shown in parts a and b of Figure 10, respectively. The lines in Figure 10a,b are least-squares fits to the data. The volume-weighted mean volume varied between 2 and 84 μm^3, which corresponds to a diameter of 1.6 and 5.4 μm, respectively. This mean was smallest for the 3% (w/w) maltodextrin concentration and largest for 5% (w/w). The sizes of the maltodextrin inclusions at 3% (w/w) maltodextrin concentration are small and nearly constant at quench temperatures between 1 and 20 °C. In contrast, the sizes of the maltodextrin inclusions increase with increasing quench temperature for 4% and 5% (w/w) maltodextrin concentrations.

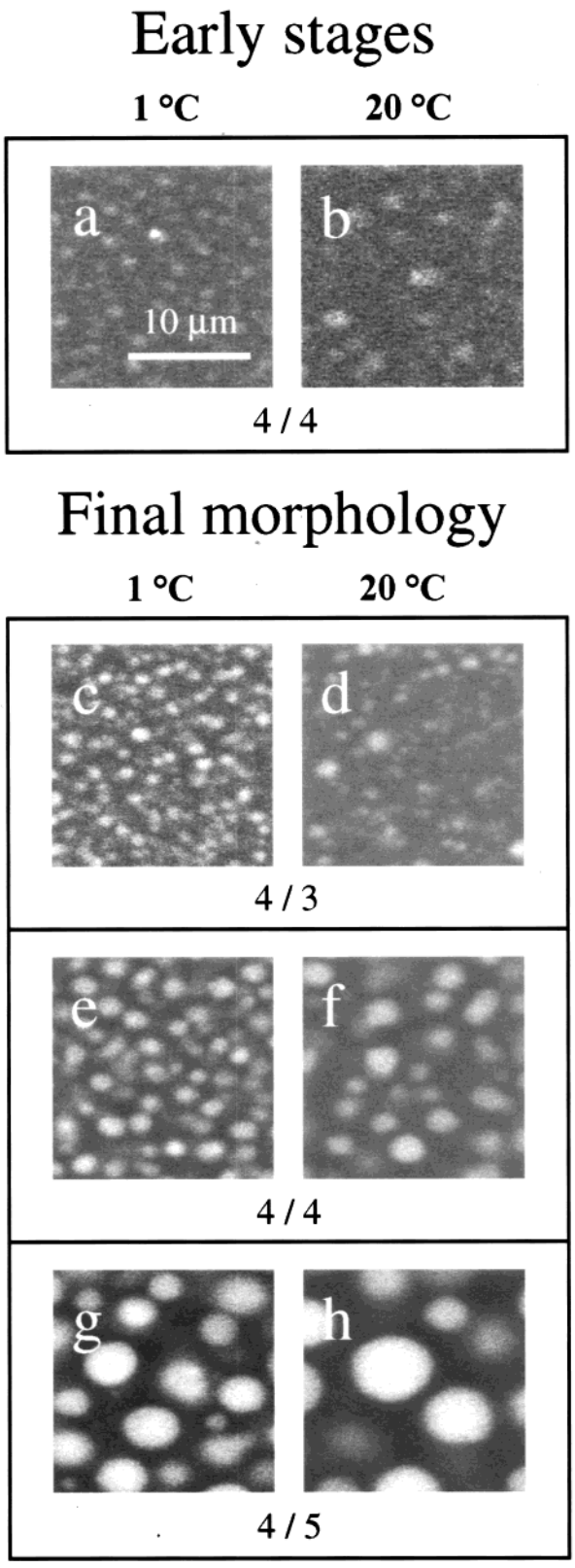

Figure 9. CLSM micrographs showing the onset of phase separation and the final morphology at 4% (w/w) gelatin concentration. Onset of phase separation: (a) 4% (w/w) maltodextrin, 1 °C; (b) 4% (w/w) maltodextrin, 20 °C. Final morphology: (c) 3% (w/w) maltodextrin, 1 °C; (d) 3% (w/w) maltodextrin, 20 °C; (e) 4% (w/w) maltodextrin, 1 °C; (f) 4% (w/w) maltodextrin, 20 °C; (g) 5% (w/w) maltodextrin, 1 °C; (h) 5% (w/w) maltodextrin, 20 °C.

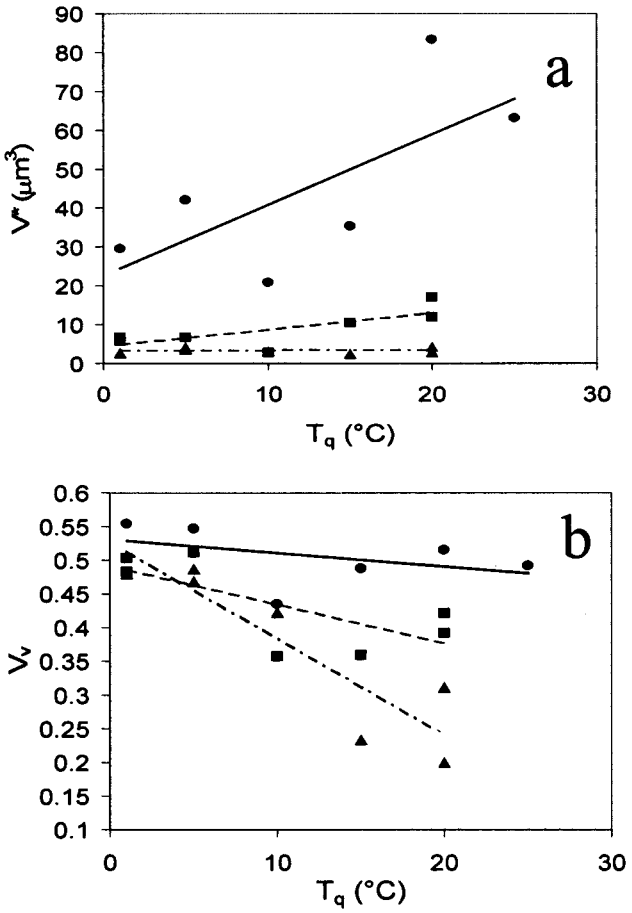

Figure 10. Stereological measurements of (a) volume-weighted mean volume (V^*) and (b) volume fraction (V_V) as a function of quench temperature. All samples measured have 4% (w/w) gelatin concentration. The dotted line represents 3% (w/w) maltodextrin concentration, the broken line represents 4% (w/w) maltodextrin concentration, and the full line represents 5% (w/w) maltodextrin concentration.

The volume fraction of the maltodextrin phase is shown in Figure 10b. This varied between 0.2 and 0.56 and was lowest for the 3% (w/w) maltodextrin concentration and highest at 5% (w/w). The volume fraction increases with decreasing quench temperature, i.e., increasing quench depth, for all maltodextrin concentrations shown in Figure 10b. The increase is greatest for the 3% (w/w) maltodextrin concentration and smallest for 5% (w/w). An increase in the volume fraction as a function of increasing quench depth has also been found in mixtures of synthetic polymers.[16,67] Figure 10 shows that high volume fractions correspond to small maltodextrin inclusions and vice versa. This means that the number of maltodextrin inclusions increases with decreasing quench temperature, which agrees with the observations in Figure 9.

The variation in the sizes and number of the maltodextrin inclusions as a function of maltodextrin concentration and quench temperature observed in Figures 9 and 10 can be explained by the kinetics of phase separation and the kinetics of gelation. The onset of phase separation is dependent on the concentration, quench depth, and the conformational ordering of gelatin. In addition, the volume fraction is mainly determined by the concentration, quench depth, and the solvent partition. The rate of gelation depends on the quench temperature at constant gelatin concentration. The phase separation thus starts with the size and number density determined by the wavelength selection mechanism and coarsens depending on the volume fraction and the driving force toward phase separation in relation to the progress of gelation. The same processes are involved in the time evolution of the morphology, although the kinetics differs.

Furthermore, the coalescence phase lasts much longer at 20 °C than at 1 °C, as the system becomes kinetically trapped more quickly at 1 °C. The longer length of the coalescence phase results in a considerable growth of the maltodextrin inclusions. The coalescence phase lasts much longer for the 5% (w/w) maltodextrin system than for the 4% (w/w) maltodextrin system at 20 °C because phase separation starts 85 s earlier, and the kinetics of gelation is approximately the same for both concentrations, owing to constant quench temperature and gelatin concentration. However, the effective concentration increases slightly in the 5% (w/w) maltodextrin system due to the decreased phase volume of the gelatin phase, which can increase the rate of gelation.

Conclusions

Confocal laser scanning microscopy (CLSM) was found to be a powerful tool for following the time evolution of the morphology during phase separation and progressing gelation of kinetically trapped gelatin/maltodextrin gels. Transmission electron microscopy (TEM) was a useful complement for examining time-dependent microstructural changes in the fine structure after gelation.

Near-symmetric quenches showed a mottled microstructure, which was taken as evidence of spinodal decomposition. The mottled microstructure coarsened through self-similar growth, and the exponent in the scaling law $L(t) \sim t^{\alpha}$ showed a crossover from $^1/_3$ to 1. Finally, a bicontinuous microstructure was formed. Secondary phase separation occurred in near-symmetric quenches at quench temperatures between 1 and 25 °C. Off-symmetric quenches were found to phase separate through spinodal decomposition, except for low maltodextrin concentrations and high quench temperatures. This quenches formed discontinuous microstructures with evenly sized, randomly distributed maltodextrin inclusions that grew through coalescence inside a continuous gelatin phase.

CLSM and TEM showed that the coarsening of the morphology at late stages of spinodal decomposition was strongly influenced by the progressing gelation. Coalescence frequency, coalescence time, coalescence type (partial coalescence and contracted flocculation), and the length of the coalescence period were determined by gelation. TEM micrographs showed that the small maltodextrin inclusions migrated through the gelatin phase to the large maltodextrin inclusions after gelation.

Observation of the time evolution of the morphology using CLSM demonstrated that the morphology at the onset of phase separation and the kinetics of phase separation in relation to the progress of gelation determined the final morphology of the gelatin/maltodextrin system. Stereological measurements of CLSM micrographs showed that the size of the maltodextrin inclusions increases, and the volume fraction decreases with increasing quench temperature. In addition, the number of the maltodextrin inclusions decreases with increasing quench temperature.

Acknowledgment. This study was carried out with financial support from TFR, the Swedish Research

Council for Engineering Science, and the Commission of the European Communities, Agriculture and Fisheries (FAIR) specific RTD program, CT 96 1015, "Mixed Biopolymers—Mechanism and Application of Phase Separation". It does not necessarily reflect its views and in no way anticipates the Commission's future policy in the area. Professor Alan Clark (Unilever Research Colworth, UK) is gratefully acknowledged for valuable comments during the preparation of the manuscript.

References and Notes

(1) Tromp, R. H.; Rennie, A. R.; Jones, R. A. L. *Macromolecules* **1995**, *28*, 4129−4138.
(2) Lorén, N.; Hermansson, A.-M.; Williams, M. A. K.; Lundin, L.; Foster, T. J.; Hubbard, C. D.; Clark, A. H.; Norton, I. T.; Bergström, E. T.; Goodall, D. M. *Macromolecules* **2001**, *34*, 289−297.
(3) Lorén, N.; Hermansson, A.-M. *Int. J Biol. Macromol.* **2000**, *27*, 250−263.
(4) Donald, A. M.; Durrani, C. M.; Jones, R. A. L.; Rennie, A. R.; Tromp, R. H. In *Biopolymer Mixtures*; Harding, S. E., Hill, S. E., Mitchell, J. R., Eds.; Nottingham University Press: Nottingham, 1995; Chapter 6, pp 99−116.
(5) Clark, A. H. In *Biopolymer Mixtures*; Harding, S. E., Hill, S. E., Mitchell, J. R., Eds.; Nottingham University Press: Nottingham, 1995; Chapter 3, pp 37−64.
(6) Lorén, N.; Langton, M.; Hermansson, A.-M. *Food Hydrocolloids* **1999**, *13*, 185−198.
(7) Bansil, R.; Lal, J.; Carvalho, B. L. *Polymer* **1992**, *33*, 2961−2969.
(8) Bansil, R.; Liao, G. *Trends Polym. Sci.* **1997**, *5*, 145−155.
(9) Sciortino, F.; Bansil, R.; Stanley, H. E.; Alstrøm, P. *Phys. Rev. E* **1993**, *47*, 4615−4618.
(10) Onuki, A.; Puri, S. *Phys. Rev. E* **1999**, *59*, 1331−1334.
(11) Nakai, A.; Shiwaku, T.; Wang, W.; Hasegawa, H.; Hashimoto, T. *Macromolecules* **1996**, *29*, 5990−6001.
(12) Jinnai, H.; Koga, T.; Nishikawa, Y.; Hashimoto, T.; Hyde, S. T. *Phys. Rev. Lett.* **1997**, *78*, 2248−2251.
(13) Jinnai, H.; Nishikawa, Y.; Morimoto, H.; Koga, T.; Hashimoto, T. *Langmuir* **2000**, *16*, 4380−4393.
(14) Ribbe, A. E.; Hashimoto, T. *Macromolecules* **1997**, *30*, 3999−4009.
(15) Binder, K.; Stauffer, D. *Phys. Rev. Lett.* **1974**, *33*, 1006−1009.
(16) Takeno, H.; Nakamura, E.; Hashimoto, T. *J. Chem. Phys.* **1999**, *110*, 3612−3620.
(17) Chesters, A. K. *Trans IchemE* **1991**, *69*, A, 259−270.
(18) Chen, H.; Chakrabarti, A. *J. Chem. Phys* **1998**, *108*, 6006−6013.
(19) Crist, B. *Macromolecules* **1996**, *29*, 7276−7279.
(20) Chakrabarti, A.; Toral, R.; Gunton, J. D. *Phys. Rev. E* **1993**, *47*, 3025−3038.
(21) Delville, J. P.; Lalaude, C.; Buil, S.; Ducasse, A. *Phys. Rev. E* **1999**, *59*, 5804−5817.
(22) Bates, F. S.; Wiltzius, P. *J. Chem. Phys.* **1989**, *91*, 3258−3274.
(23) Gunton, J. D.; San Miguel, M.; Sahni, P. S. In *Phase Transitions and Critical Phenomena*; Domb, C., Lebowitz, J. L., Eds.; Plenum Press: New York, 1983; Vol. 8, pp 267−466.
(24) Aksimentiev, A.; Moorthi, K.; Holyst, R. *J. Chem. Phys.* **2000**, *112*, 6049−6062.
(25) Bray, A. J. Scottish Universities Summer School in Physics 53 1999 St. Andrews; *Soft and Fragile Matter*; Cates, M. E., Evans, M. R., Eds.; 1999; pp 205−236.
(26) Siggia, E. D. *Phys. Rev. A* **1979**, *20*, 595−605.
(27) Furukawa, H. *Phys. Rev.* **1985**, *31*, 1103.
(28) Lifshitz, I. M.; Slyozov, V. V. *Phys. Chem. Solids* **1961**, *19*, 35.
(29) Wagner, C. *Z. Electrochem.* **1961**, *65*, 581.
(30) Binder, K.; Stauffer, D. *Adv. Phys.* **1976**, *25*, 343.
(31) Tanaka, H. *J. Chem. Phys.* **1995**, *103*, 2361−2364.
(32) Tanaka, H. *Phys. Rev. Lett.* **1994**, *72*, 1702−1705.
(33) Garnier, C.; Bourriot, S.; Doublier, J.-L. In *Gums and Stabilisers for the Food Industry 9*; Williams, P. A., Phillips, G. O., Eds.; The Royal Society of Chemistry: Cambridge, 1998; pp 247−256.
(34) De Belder, A. N.; Granath, K. *Carbohydr. Res.* **1973**, *30*, 375.
(35) Gundersen, H. J. G. *J. Microsc.* **1977**, *111*, 219.
(36) Gundersen, H. J. G.; Bendtsen, T. F.; Korbo, L.; Marcussen, N.; Møller, A.; Nielsen, K.; Nyengaard, J. R.; Pakkenberg, B.; Sørensen, F. B.; Vesterby, A.; West, M. J. *APMIS* **1988**, *96*, 379.
(37) Weibel, E. R. *Stereological Methods. Theoretical Foundations*; Academic Press: New York, 1980; Vol. 2.
(38) Piculell, L.; Lindman, B. *Adv. Colloid Interface Sci.* **1992**, *41*, 149−178.
(39) Koningveld, R.; Stockmayer, W. H.; Nies, E. *Polymer Phase Diagrams*; Oxford University Press: Oxford, 2001.
(40) Copetti, M. I. M.; Elliott, C. M. *Mater. Sci. Technol.* **1990**, *6*, 273−283.
(41) Chakrabarti, A. *Phys. Rev. B* **1992**, *45*, 9620.
(42) Hashimoto, T.; Itakura, M.; Hasegawa, H. *J. Chem. Phys.* **1986**, *85*, 6118.
(43) Jones, R. A. L.; Richards, R. W. *Polymer at Surfaces and Interfaces*; Cambridge University Press: Cambridge, 1999.
(44) Cahn, J. W. *J. Chem. Phys.* **1965**, *42*, 93.
(45) Lundin, L.; Norton, I. T.; Foster, T. J.; Williams, M. A. K.; Hermansson, A.-M.; Bergström, E. In *Gums and Stabilisers for theFood Industry 10*; Williams, P. A., Philips, G. O., Eds.; The Royal Society of Chemistry: Cambridge, 2000; pp 167−180.
(46) Verhaegh, N. A. M.; van Duijneveldt, J. S.; Dhont, J. K. G.; Lekkerkerker, H. N. W. *J. Chem. Phys* **1996**, *102*, 409.
(47) Tuinier, R.; Dhont, J. K. G.; De Kruif, C. G. *Langmuir* **2000**, *16*, 1497−1507.
(48) Djabourov, M.; Maquet, J.; Theveneau, H.; Papon, P. *Br. Polym. J.* **1985**, *17*, 169−174.
(49) Chan, P. K.; Rey, A. D. *Macromolecules* **1997**, *30*, 2135−2143.
(50) Tanaka, H.; Yokokawa, H.; Abe, H.; Hayashi, T.; Nishi, T. *Phys. Rev. Lett.* **1990**, *65*, 3136.
(51) Binder, K.; Billotet, C.; Mirold, P. *Z. Phys.* **1978**, *B30*, 183−195.
(52) McGuire, K. S.; Laxminarayan, A.; Martula, D. S.; Lloyd, D. R. *J. Colloid Interface Sci.* **1996**, *182*, 46−58.
(53) Fortélny, I.; Živný, A. *Polymer* **1995**, *36*, 4113−4118.
(54) Russo, A. P.; Nauman, E. B. *Polym. Mtrl. Sci. Eng./Proc. ACS Div. Polym. Mtrl. Washington* **1998**, *79*, 175−176.
(55) Cavanaugh, T. J.; Nauman, E. B. *J. Polym. Sci., Part B: Polym. Phys.* **1998**, *36*, 2191−2196.
(56) Perrot, F.; Guenoun, P.; Baumberger, T.; Beysens, D.; Garrabos, Y.; Le Neindre, B. *Phys. Rev. Lett.* **1994**, *73*, 688.
(57) Tambe, D. E.; Sharma, M. M. *J. Colloid Interface Sci.* **1991**, *147*, 137−151.
(58) Nakai, A.; Shiwaku, T.; Hashimoto, T. *Macromolecules* **1986**, *19*, 3008.
(59) Sappelt, D.; Jäckle, J. *Physica A* **1997**, *240*, 453−479.
(60) Binder, K. In *Materials Science and Technology*; Haasen, P., Ed.; VCH: Weinheim, 1991; Vol. 5, Chapter 7.
(61) Inoue, T. *Prog. Polym. Sci.* **1995**, *20*, 119−153.
(62) Clarke, N.; Mcleish, T. C. B.; Jenkins, S. D. *Macromolecules* **1995**, *28*, 4650−4659.
(63) Williams, R. J. J.; Rozenberg, B. A.; Pascault, J.-P. *Adv. Polym. Sci.* **1997**, *128*, 95−156.
(64) Tanaka, H.; Araki, T. *Phys. Rev. Lett.* **1998**, *81*, 2, 389−392.
(65) Cavanaugh, T. J.; Buttle, K.; Turner, J. N.; Nauman, E. B. *Polymer* **1998**, *39*, 3611−3621.
(66) Binder, K.; Frisch, H. L. *J. Chem. Phys.* **1984**, *81*, 2126.
(67) White, W. R.; Wiltzius, P. *Phys. Rev. Lett.* **1995**, *75*, 3012−3015.

MA010722Q